Controlled production of eco-friendly emulsions using direct and premix membrane emulsification

Graphical Abstract (for review)

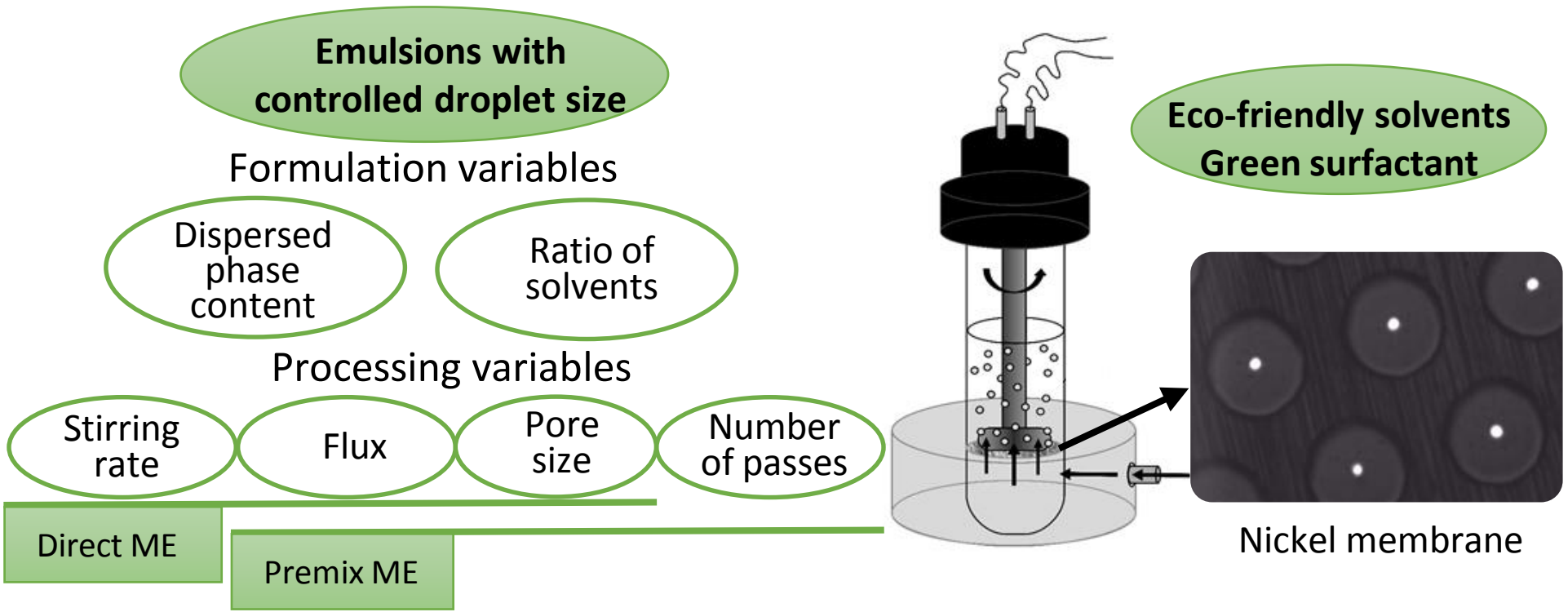

Highlights

- Production of size-controlled eco-friendly emulsions was achieved with ME.
- The most uniform emulsion was obtained with pure d-limonene.
- The addition of AMD-10 caused a decrease in droplet size at the same energy input.
- Droplet size lower than the pore size was obtained in premix ME.
- Emulsion with a dispersed phase content of 40 wt% showed viscoelastic properties.

Controlled production of eco-friendly emulsions using direct and premix membrane emulsification

Jenifer Santos[1], Goran T. Vladisavljević[2*], Richard G. Holdich[2], Marijana M. Dragosavac[2], José Muñoz[1].

[1]Reología Aplicada. Tecnología de Coloides. Departamento de Ingeniería Química. Facultad de Química. Universidad de Sevilla c/ P. García González, 1, E41012, Sevilla Spain.

[2]Chemical Engineering Department, Loughborough University, Loughborough, Leicestershire LE11 3TU, UK.

*Corresponding author. Tel.: +44 (0)1509 222518. *E-mail address*: G.Vladisavljevic@lboro.ac.uk

Abstract

Eco-friendly O/W emulsions were produced by membrane emulsification using nickel membrane consisting of hexagonal arrays of cylindrical pores of 10 or 20 µm diameter and 200 µm spacing. The dispersed phase was a mixture of N,N-dimethyldecanamide (AMD-10™) and d-limonene containing 0-35 wt% AMD-10™ in the dispersed phase and the continuous aqueous phase was 3 wt% polyoxyethylene glycerol fatty acid ester (Levenol® C-201). In direct membrane emulsification, the droplet-to-pore size ratio was 1.5-4.6 and the most uniform droplets were obtained with pure d-limonene at a stirrer speed of 620 rpm, corresponding to the peak shear stress on the membrane surface of 7 Pa. In premix membrane emulsification, the median droplet diameter decreased with increasing the transmembrane flux and was smaller than the pore size

at the flux above 2000 L m^{-2} h^{-1}. The droplet size was 6 µm after two passes through the membrane with a pore diameter of either 10 or 20 µm. The viscosity of emulsions with 30 wt% was not influenced by the shear rate but an emulsion with a dispersed phase content of 40 wt% showed shear thinning behaviour and viscoelastic properties. The produced emulsions can be used as environmentally friendly matrices for incorporation of agrochemical actives.

Keywords: Membrane Emulsification, Stirred Cell, Eco-Friendly Emulsions, Green Solvents, Agrochemicals, Emulsion Rheology.

Introduction

The task of product engineering is to design products of desirable features for given applications. All properties are the result of certain physical and chemical characteristics of the product, which are determined by the choice of the formulation and processing conditions. Many important properties of emulsions are largely determined by structural parameters such as volume ratio of the phases, particle size distribution and mean particle size (Schubert et al., 2003). Production of emulsion-based systems with specific physicochemical and functional properties often requires control over the particle size distribution (PSD) (McClements, 2005, Santos et al., 2011).

Conventional emulsification devices such as colloid mills, rotor-stator mixers, high-pressure homogenizers and ultrasonic homogenizers offer limited flexibility in terms of PSD. Recently, membrane emulsification (ME) has received much attention due to its

ability to control the mean droplet size over a wide range together with the ability to provide a narrow size distribution (Kosvintsev et al., 2005). Low energy consumption lies at the heart of sustainable and socially responsible society (Cussler and Moggridge, 2011). The reduction in energy requirements by using ME is very significant when compared with other homogenization processes. In fact, energy densities required to achieve a mean droplet size of 1-10 μm using premix ME typically range from 10^4 to 10^6 Jm^{-3}, while those of rotor-stator devices and high pressure homogenizers range from 10^6 to 10^8 Jm^{-3} (Karbstein and Schubert, 1995). In addition, the ability to form uniform dispersions with a technique that can be scaled from small scale to industrial production makes the process very attractive (Peng and Williams, 1998); cross flow membrane emulsification being the technique of choice for scaling-up.

Two main types of ME processes have been developed: direct ME involving the permeation of pure dispersed phase through a microporous membrane into agitating or recirculating continuous phase and premix ME involving the passage of previously prepared coarse emulsion through the membrane (Charcosset et al., 2004). Premix ME provides several advantages over direct ME: (i) the dispersed phase flux is higher, so the time required for the production is very short; (ii) the mean droplet-to-pore size ratios are smaller than in direct ME. In direct ME, the mean droplet-to-pore size ratio can range between 2 and 50 (Ma, 2003, Yuan et al., 2009, Zhou et al., 2009), but it is often below 10. In premix ME, the mean droplet-to-pore size ratio is typically between 0.6 and 2 (Vladisavljević et al., 2006); (iii) the process parameters are easier to control than in direct ME. One of the disadvantages of premix ME is a higher emulsion polydispersity compared to direct ME.

71 Premix ME has been applied using a wide range of membranes, such as Shirasu Porous
72 Glass (SPG) membrane (Suzuki et al., 1996), polycarbonate (Yafei et al., 2009), nylon
73 and nitrocellulose polymeric membranes (Ramakrishnan et al., 2012), and nickel
74 microsieves with rectangular and square membranes (Nazir et al., 2011, 2013). Typical
75 laboratory devices for ME are SPG micro kits (Kukizaki and Goto, 2007) and Micropore
76 Dispersion Cell (MDC) (Kosvintsev et al., 2005). Although MDC has been widely used in
77 direct ME, so far there are no published studies on premix ME in MDC.

78 In recent years, there has been an increasing interest in using the so-called green
79 solvents due to the need to replace traditional petrochemical organic solvents by more
80 environmentally friendly solvents derived from agricultural crops (Anastas and
81 Wagner, 1998). N,N-dimethyldecanamide (AMD-10^{TM}) is considered as a safe
82 biosolvent, according to the Environmental Protection Agency in 2005 and has
83 excellent solubilizing properties towards agrochemical actives. Therefore, AMD-10^{TM} is
84 a suitable solvent for agrochemical use (Hofer and Bigorra, 2007), that imposes
85 minimal risk to the farmers while satisfying the needs of customers, which is a principal
86 aim of the product design (Brokel et al., 2007).

87 D-limonene, a naturally occurring hydrocarbon, is a cyclic monoterpene, which is
88 commonly found in the rinds of citrus fruits such as grapefruit, lemon, lime, and in
89 particular, oranges. D-limonene exhibits good biodegradability, hence it may be used
90 as a direct substitute for toxic organic solvents (Walter, 2010, Medvedovici et al.,
91 2012). These two solvents can meet the ever-increasing performance, safety and
92 environmental demands of 21st century solvents. In this study, mixtures of d-limonene
93 and AMD-10^{TM} will be used as a dispersed phase. The use of these solvent blends as a

dispersed phase instead of common organic solvents and vegetable oils could represent a challenge for the size control in ME, due to their distinct physical properties, such as low viscosity, low interfacial tension and a medium solubility in water of AMD-10^{TM} (340 mg L^{-1}).

In addition, environmentally friendly surfactants have also attracted significant interest recently. Polyoxyethylene glycerol esters derived from cocoa oil are non-ionic surfactants obtained from a renewable source, which fulfil the environmental and toxicological requirements for eco-friendly foaming and/or emulsifying agents (Castán and González, 2003). Their use as green surfactants in detergents and personal care products is disclosed in several patents (Lutz, 2006; Denolle, 2011). Levenol® C-201 and Levenol® H&B are commercial polyoxyethylene glycerol esters. The former was found to be more surface active at the biocompatible α-pinene/water interface than Levenol H&B, its counterpart with a lower number of oxyethylene groups (Trujillo-Cayado et al., 2014a and 2014b).

The main objective of this work was to produce O/W eco-friendly emulsions with a controlled mean droplet size using ME. For the first time, premix ME has been performed in a Micropore Dispersion Cell (MDS) using micro-engineered membranes with circular pores. The operation procedure, formulation, pore size, and process parameters were optimized in order to obtain finer emulsions with low energy inputs. These emulsions may be used as matrices for incorporation of active agrochemical ingredients. This study is a contribution towards the development of new emulsion products, which may fulfil the customers' needs as well as the requirements of the related industries.

Experimental

2.1. Materials

N,N Dimethyl Decanamide (Agnique AMD-10^{TM}) was kindly provided by BASF. D-Limonene was supplied by Sigma Chemical Company. The dispersed phase was a mixture of AMD-10^{TM} and d-limonene containing 0, 25, or 35 wt% of AMD-10^{TM}. The dispersed phase content in the prepared emulsions was 30 wt% in all experiments except those reported in Figure 8, where it was 5-40 wt %.

The continuous phase was 3 wt% Levenol® C-201 and 0.1 wt% antifoam agent dissolved in deionized water. Levenol® C-201 is a nonionic surfactant derived from cocoa oil, received as a gift from KAO Chemicals. It is a trade name of glycereth-17 cocoate (HLB:13), which is an ester of coconut acid and a polyethylene glycol ether of glycerol containing an average of 17 ethylene oxide units per molecule. RD antifoam emulsion (DOW CORNING®) was used as antifoaming agent. This commercial product consists of an aqueous solution containing polydimethyl siloxane (<10 wt%) and dimethyl siloxane, hydroxyl-terminated (<10 wt%).

2.2 Membrane and membrane module

The emulsions were obtained using a Micropore Dispersion Cell (MDS), a stirred cell with a flat disc membrane under the paddle stirrer shown in Figure 1. Both stirred cell and membranes were supplied by Micropore Technologies Ltd. (Loughborough, UK). The agitator was driven by a 24 V DC motor (INSTEK Model PR 3060) and paddle rotation speed was controlled by the applied voltage.

The membranes used were nickel membranes containing uniform cylindrical pores with a diameter of d_p= 10 µm or d_p= 20 µm and a spacing of L= 200 µm. The membranes were fabricated by the LIGA process, which involves galvanic deposition of nickel onto a template formed by photolithography and etching. Perfectly ordered hexagonal arrays of pores with one pore at the centre of each hexagonal cell can be seen on the micrographs in Figure 2.

The porosity of a membrane with regular hexagonal pore array is given by:

$$\varepsilon = \frac{\pi}{2\sqrt{3}}\left(\frac{d_p}{L}\right)^2 \qquad (1)$$

For the membranes used in this work, the porosity calculated from Eq. (1) is 0.26% and 0.90% for d_p= 10 and 20 µm, respectively. The effective cross-sectional area of the whole membrane is 8.5 cm^2, which is significantly greater than 1.4 cm^2, which was the membrane area used in previous premix ME studies with microsieve membranes (Nazir et al., 2011, 2013).

2.3. Emulsion production

2.3.1. Direct membrane emulsification

Dispersed phase was injected through the membrane using a syringe pump (Secondary Dual Pump, World Precision Instruments, Sarasota, Florida) at the constant flow rate of 110-910 mL h^{-1}, corresponding to the dispersed phase flux of 129-1070 L m^{-2} h^{-1} (See Figure 1A). The stirring speed was fixed at 400-1200 rpm. Once the desired amount of oil had passed though the membrane, both the pump and the agitator were switched off and the droplets were collected and analyzed. The membrane was cleaned with 4

160 M NaOH in an ultrasonic bath for 5 min followed by treatment in 2 wt% citric acid for 5
161 min.

162 **2.3.2. Premix membrane emulsification**

163 The mixture of solvents and the continuous phase was first premixed for one minute
164 using a magnetic bar to produce a coarse emulsion with large droplets. This coarse
165 emulsion was then injected 1-3 times through the membrane using a syringe pump
166 (Model 11 Plus, Harvard Apparatus) at the constant flow rate of 110-910 mL h^{-1},
167 corresponding to the flux of 129-1070 L m^{-2} h^{-1} (See figure 1B). The membrane was not
168 cleaned between the passes. The emulsion samples obtained after each pass were
169 collected and analysed.

170 **2.4. Droplet size distribution measurements**

171 PSD of oil droplets was determined by static laser light scattering (laser diffraction)
172 using Mastersizer 2000 (Malvern, Worcestershire, United Kingdom). All measurements
173 were repeated three times for each sample.

174 The mean droplet diameter was expressed as the volume median diameter d(v,0.5),
175 which is the diameter corresponding to 50 vol% on the cumulative distribution curve.
176 The relative span of a drop size distribution was used to express the degree of drop
177 size uniformity (see Eq. 2).

178 $$span = \frac{[d(v,0.9) - d(v,0.1)]}{d(v,0.5)} \quad (2)$$

179 **2.5. Rheological measurements**

Rheological experiments were conducted with AR 1000 controlled-stress rheometer (TA instruments, USA), equipped with a cone-plate of 60 mm diameter and 1 degree. Flow curves were generated from 0.05 Pa to 1 Pa at 20°C. Small amplitude oscillatory shear tests were carried out for the emulsion containing 40 wt % of dispersed phase. The frequency sweep was carried out in the 20-0.5 rad s^{-1} angular frequency range at shear stress amplitude of 0.05 Pa. This was previously determined by conducting oscillatory stress sweeps at three different frequencies, namely 0.63 rad s^{-1}, 6.3 rad $s^{-1}$and 18.9 rad s^{-1}. All measurements were repeated 3 times with each emulsion. Sampling from the top part of the container in contact with air was avoided.

3. Results

3.1. Reproducibility of experimental data

Figure 3 shows PSD curves for the emulsions prepared using direct ME with 10 μm membrane (Fig. 3A) and premix ME with 20 μm membrane (Fig. 3B). In each case, the dispersed phase contained 25 wt% AMD-10™ and 75 wt% d-limonene. Replicated runs 1, 2 and 3 in Fig. 3A were performed on the same day, while run 4 was done in two days, after several other experiments had been performed in the meantime. PSD for all replicates was very similar, which indicates that the membrane cleaning procedure was robust and successful. The average D(v,0.5) value was (28.79 ± 1.37) μm and span was 1.35 ± 0.03, where the error margins were calculated as one standard deviation away from the mean. There is no difference between a new and used membrane provided that a new membrane was treated with a wetting agent to render the surface hydrophilic (Fig. 3A). The new membrane that was not treated with wetting agent exhibited the broadest particle size distribution in Fig. 3A.

In addition, PSD for the emulsions prepared by premix ME did not change substantially in the experiments repeated 3 times under constant experimental conditions (Fig 3B). The average D(v,0.5) value was (23.16 ± 1.85) μm and span was 1.78 ± 0.09. The reproducibility of the results in direct ME was better than that in the premix process, probably because the PSD of the coarse emulsion was not exactly the same in all premix ME runs. In both processes, bimodal distributions were obtained and PSD was more uniform in the samples prepared by direct ME.

3.2 Laser diffraction measurements

3.2.1. Direct Membrane Emulsification

Figure 4 shows PSD for the emulsions prepared by direct ME at 620 rpm and 600 L m^{-2} h^{-1} with a 10 μm and 20 μm membrane as a function of the solvent ratio in the dispersed phase. An increase in the content of AMD-10^{TM} in the dispersed phase caused a shift of the distribution towards smaller droplet sizes and the distribution became wider, as evidenced by higher span values (Table 1). This could be due to the low interfacial tension of the solvent blends compared to pure d-limonene (Table 2). The interfacial tension force is the main force resisting the drag force and holding a growing droplet at the membrane surface. By decreasing the interfacial tension, the droplets detach sooner from the membrane surface and the resultant droplet size is smaller. In addition, AMD-10^{TM} is more polar solvent than d-limonene (the solubility of AMD-10^{TM} and D-Limonene in water is 340 and 13.8 mg L^{-1}, respectively), which means that the solvent blends have a higher affinity towards the hydrophilic membrane surface than pure d-limonene. The PSD curves for pure limonene are monomodal, suggesting that the membrane was not wetted by pure d-limonene during

emulsification. In addition, the impact of the pore size on the mean droplet size was very substantial for the pure limonene emulsions and negligible for the 25/75 emulsions. This may be related to the low interfacial tension of the mixture that is the crucial property to achieve low droplet size (Santos et al., 2014). The subsequent experiments will be done using the 25/75 solvent mixture which is a compromise between a need to obtain a narrow distribution and to replace as much d-limonene as possible by a cheaper AMD-10^{TM} solvent.

Figure 5 shows the effect of stirring speed on the droplet size distribution for 25/75 emulsions prepared with a 10 μm membrane at the oil flux of 600 L m^{-2} h^{-1}. The increase of stirring speed caused the PSD curves to shift toward smaller droplet sizes. In addition, the volume median diameter decreased with increasing the stirring speed (Fig. 6), which was due to an increase of the drag force acting on the droplets. The same stirring rate vs. droplet size relationship was reported by Kosvintsev et al. (2005) and Stillwell et al. (2007) for sunflower O/W emulsions. The droplet size showed large variations with stirring speed up to 620 rpm, corresponding to average shear stress at the membrane surface of 6.25 Pa. However, the effect was less pronounced at the higher stirring speeds, when the volume median diameter virtually reached its asymptotic value. Figure 6 also provides a comparison of experimental drop size and model prediction at different stirring speeds. The shear-capillary model used in this work (see Appendix A) does not recognise the dispersed phase flux as having a contribution to the formed droplet size. Therefore, the model should represent the smallest droplet size that can be produced for a given set of operating conditions. It could explain why the model fits the experimental data best at high stirring speeds,

where the droplet formation times are very short due to high drag forces exerted on the droplets by the stirrer (Dragosavac et al., 2008).

Figure 6 also shows the influence of stirring speed on the span values for the emulsions prepared at 600 L m^{-2} h^{-1} with a 10 µm membrane. The higher span values obtained above 620 rpm could be attributed to more significant deformation of the droplets on the membrane surface before detachment due to high shearing, which can lead to more pronounced droplet interactions with the membrane surface and membrane wetting. The optimal rotational speed with regard to droplet size uniformity was 620 rpm, which corresponded to the peak shear stress on the membrane surface of 7 Pa.

Figure 7 shows D(v,0.5) and span as a function of transmembrane flux for the emulsions prepared with a 10 and 20 µm membrane. The rotational speed was kept at the optimal value of 620 rpm. For both pore sizes, an increase in the transmembrane flux led to an increase in the mean droplet size, while span did not show significant variations. As the transmembrane flux is increased, the drop grows faster and the interface cannot be stabilised fast enough by adsorbed emulsifier molecules. In addition, at higher transmembrane fluxes a higher amount of oil will flow into the growing drop during pinch off. This effect was more significant up to 400 L h^{-1} m^{-2} and then the droplet size tended to stabilize, probably due to droplet-droplet interactions on the membrane surface that restricted further droplet growth (Egidi et al., 2008).

The influence of pore size on D(v,0.5) was insignificant for the emulsions containing AMD-10™ in the dispersed phase. However, span increased with an increase in the pore size. Therefore, the optimum conditions for direct ME in this work were: a pore size of 10 µm, a transmembrane flux of 129 L m^{-2} h^{-1} and a stirrer speed of 620 rpm.

Figure 8 shows the effect of dispersed phase content on D(v,0.5) for 25/75 emulsions prepared by direct ME at 129 L m^{-2} h^{-1} and 620 rpm using a 10 µm membrane. The surfactant/oil ratio was kept at 0.10 (w/w) in all samples. The volume median diameter decreased with increasing the dispersed phase content in the emulsion. For a given surfactant/oil ratio (R=0.10), when the dispersed phase content is increased, the surfactant concentration in the continuous phase also increases, leading to the higher viscosity of the continuous phase, η_c. It has been reported that the viscosity of the continuous phase significantly affects the droplet size obtained in rotor stator homogenizers and in direct ME. It is stated that an increase in η_c will lead to an increase of the drag force acting on the forming droplets at the same stirring speed producing smaller droplets (Vankova et al., 2007, Dragosavac et al., 2008).

3.2.2. Premix membrane emulsification

Figure 9A illustrates the effect of transmembrane flux on the PSD of emulsions produced by premix ME with a 10 µm membrane. Injection of pre-mix through the membrane led to reduction in the droplet size and modification of the PSD compared to that of the pre-mix.

An increase in the transmembrane flux caused a shift of the PSD curves towards lower droplet sizes. As a result of energy input brought by fluid flow, large oil drops in the coarse emulsion were deformed in the pores and broken up into smaller droplets (Van Aken, 2002). A reduction in drop size occurred as a result of various disruptive forces, such as shear and extensional forces, interfacial tension effects (Rayleigh and Laplace instabilities) and impact forces due to droplet-droplet and droplet-pore wall interactions (Vladisavljević et al., 2004 and 2006, Cheetangdee et al., 2011). Here,

droplet-pore wall interactions are probably less significant than in SPG membrane, due to shorter pore lengths as a result of non-tortuous and non-interconnected pores and small membrane thickness. The wall shear stress τ_p in cylindrical non-tortuous pores with a diameter of d_p is given by (Vladisavljević et al., 2006b): $\tau_p = 8\eta_c J/(\varepsilon d_p)$, where ε is the membrane porosity defined by Eq. (1) and J is the transmembrane flux. Hence, τ_p increases with increasing J, which results in more intensive droplet break-up, as shown in Figs. 9 and 10. The droplet size can also be reduced by increasing number of passes through membrane, as shown in Figure 9B, due to additional amount of energy added to the system (Vladisavljević et al., 2006). The same trend was observed in this work, although larger droplets were still present in the product emulsion after two passes (Fig. 9B), probably due to partial droplet re-coalescence. Due to bimodal PSDs, the span values were 1.5-6 (the data not shown here). The fraction of larger droplets (d>10 μm) can be reduced by implementing three passes, as can be seen from the PSD curves at 706 L m^{-2} h^{-1} in Fig. 9B.

Figure 10 shows the effect of transmembrane flux on the volume median diameter of the product emulsions after 1-3 membrane passes. The transmembrane pressure, Δp is equivalent to energy input per unit volume, E_V and can be expressed as follows: $E_V = \Delta p = J(R_m + R_f)$, where R_m and R_f is the hydraulic resistance of the clean membrane and fouling layer, respectively. The fouling resistance occurs due to accumulation of oil drops on the upstream side of the membrane (external fouling) and inside the pores (internal fouling) (Vladisavljevic et al., 2004). The mean Sauter diameter of an emulsion produced in mechanical emulsification device exponentially decreases with increasing energy input per unit volume (Karbstein and Schubert,

1995): $D_{3,2} = CE_V^{-b}$, where C and b are constants whose values depend on the physical properties of the phases. If the total hydraulic resistance is constant, the above equation can be simplified to $D_{3,2} \propto J^{-b}$. Therefore, the higher the flux, the lower the resultant droplet size, which agrees with the results in Fig. 10. The same behaviour was observed by Suzuki et al. (1996 and 1998) in premix ME with SPG and PTFE membranes.

D(v,0.5) was less than 10 μm (the pore size) after two passes through the membrane irrespective of the flux and even after a single pass at the flux of 2118 L m^{-2} h^{-1}. Large droplets of a pre-mix are squeezed as they pass through the pores due to elongational forces. At high flux values, a deformed droplet remains elongated after it exits the pore, due to high velocity of the continuous phase relative to that of the dispersed phase (van der Zwan et al., 2006). The resulting long droplet filament is subjected to Plateau-Rayleigh instability due to perturbations on its interface, which leads to jet fragmentation into very fine droplets, typically smaller than the pore size. At low fluxes, a squeezed droplet re-emerges on the downstream side of the membrane acquiring a dumbbell shape. The droplet does not form a long cylinder, since the flow rate of the continuous phase is insufficient and thus, Plateau-Rayleigh instability is not relevant (van der Zwan et al., 2006). The droplet is disrupted due to Laplace instability caused by the difference in capillary pressure between the dispersed phase in the neck region inside the pore and the dispersed phase before and after the pore (in hemispherical ends).

Figures 11 (A) and (B) show the effect of transmembrane flux and number of passes through the membrane, respectively, on the PSD for emulsions prepared using a 20

μm membrane. As expected, the smallest droplets were obtained after two passes at 2118 L m^{-2} h^{-1} (due to the highest energy input) and the biggest droplets were produced at 350 L m^{-2} h^{-1} after single pass.

Figure 12 shows the effect of transmembrane flux and number of passes on for the 20 μm pore size. The D(v,0.5) value after first pass at 2118 L m^{-2} h^{-1} was 15 μm and was higher than that for the 10 μm pore size. At the constant flux, flow velocity in the membrane pores is lower for larger pores, due to 3.5 times higher membrane porosity, leading to less intensive droplet break-up. The volume median diameter after two passes levelled off at about 6 μm and was similar to the limiting D(v,0.5) value for the 10 μm pore size after two passes. However, span values for 20 μm pore size membrane were lower than those for the 10 μm pore size (data not shown). Therefore, in premix ME more uniform emulsion droplets were produced with the higher pore size, as opposed to direct ME.

3.3. Rheological measurements

Figures 13A and 13B show flow properties of 30 wt% emulsions prepared by direct and premix ME, respectively, as a function of transmembrane flux and number of passes. In both cases, the pore size of the membrane was 10 μm. All samples with 30% dispersed phase exhibited Newtonian behaviour with the flow curves fitting fairly well to the Newtonian law. Hence, viscosities of these emulsions are not influenced by shear rate.

Increasing the stirring speed increases the viscosity of the samples, which supports laser diffraction results. An increase of transmembrane flux and number of passes led to an increase of viscosity. In addition, the emulsions prepared by premix ME showed higher viscosities than the ones obtained by direct process. These results are in good

364 correlation with the mean droplet diameters observed by laser diffraction. Clearly,
365 emulsions with a dispersed phase content of 30 wt% did not possess enough internal
366 structure to show shear thinning behaviour or viscoelastic properties.

367 By contrast, an emulsion with a dispersed phase content of 40 wt% exhibited shear
368 thinning behaviour and viscoelastic properties. Measurable viscoelastic responses
369 could not be obtained below 40 wt% dispersed phase. Figure 13C shows mechanical
370 spectrum of a 40 wt% emulsion produced by direct ME at 620 rpm and 129 L m^{-2} h^{-1}.
371 The loss modulus G'' was higher than the storage modulus G' at every frequency. This
372 behaviour is typical in viscoelastic liquids (tan δ >1) (Mezger, 2006). Emulsions with
373 viscoelastic properties usually show better stabilities against creaming than the non-
374 viscoelastic emulsions (Barnes, 1994).

375

376 **Conclusions**

377 The production of eco-friendly emulsions with a median droplet diameter ranging from
378 21 to 69 μm has been demonstrated using direct and premix membrane emulsification
379 (ME) in a simple paddle-bladed stirred cell. An increase of the content of AMD-10™
380 solvent in the dispersed phase caused a decrease in the mean droplet size and
381 deterioration of the droplet size distribution, probably due to lower interfacial tension
382 and higher polarity of the solvent blend compared to pure d-limonene. In direct ME,
383 the mean droplet size decreased with increasing the stirring speed and decreasing the
384 transmembrane flux. The droplet-to-pore size ratio was 2.2-4.6 and 1.5-3.5 for the
385 membrane with a pore size of 10 and 20 μm, respectively. The minimum droplet-to-
386 pore size ratio of 1.5 was smaller than 3 reported in direct ME with SPG membrane,

probably due to very low interfacial tension of 1 mN/m when 25/75 solvent mixture was used. The most uniform droplets were obtained at the flux of 600 L m^{-2} h^{-1} and the stirrer speed of 620 rpm, which corresponded to the peak shear stress on the membrane surface of 7 Pa. For a constant surfactant/oil ratio (*R*) of 0.10, the mean droplet size decreased with increasing the dispersed phase content in the emulsion.

In premix ME, the mean droplet size exponentially decreased with increasing transmembrane flux from an initial value greater than 50 µm in a pre-mix to a final value lower than the pore size in the emulsions processed at the flux above 2000 L m^{-2} h^{-1}. The mean droplet size was additionally reduced using two or three passes through the membrane, but the particle size distribution was relatively broad. A lower transmembrane flux and smaller number of passes were needed to achieve the same droplet size reduction as with SPG membrane of the same pore size, probably due to smaller interfacial tension in this work. The effect of pore size on the mean droplet size was more pronounced in premix than in direct ME. This work demonstrates that premix ME with only two passes through nickel micro-engineered membrane enables to obtain O/W emulsions with very small mean droplet sizes compared to the pore size. The mean droplet size lower than 6 µm was achieved using both 10 and 20 µm membrane, but more uniform droplets were obtained with a 20 µm membrane.

O/W emulsions with a dispersed phase content of 40 wt% showed viscoelastic properties, due to structuration in the emulsion. On the other hand, O/W emulsions with a dispersed phase content of 30 wt% exhibited Newtonian behaviour with the viscosity values in a good correlation with the mean droplet sizes.

Acknowledgements

The financial support received (Project CTQ2011-27371) from the Spanish Ministerio de Economía y Competitividad, the European Commission (FEDER Programme) and from V Plan Propio Universidad de Sevilla is kindly acknowledged.

The authors are also grateful to BASF and KAO for providing materials for this research.

Appendix A

For predicting the drop size of the dispersed phase, a force-balance model (Dragosavac et al., 2008) has been used here.

The shear stress τ at the membrane surface varies with the radial distance from the stirrer axis, r, according to the equations (Nagata, 1975):

For $r < r_{trans}$ $$\tau = 0.825\, \eta_c \omega r \frac{1}{\delta} \quad (3)$$

For $r > r_{trans}$ $$\tau = 0.825\, \eta_c \omega r_{trans} \left(\frac{r_{trans}}{r}\right)^{0.6} \frac{1}{\delta} \quad (4)$$

where r_{trans} is the transitional radius, i.e. the radial distance where the shear stress is greatest:

$$\mathrm{r_{trans}} = 1.23 \frac{D}{2}\left(0.57 + 0.35\, \frac{D}{T}\right)\left(\frac{b}{T}\right)^{0.036} n_b^{0.116} \frac{Re}{1000 + 1.43\, Re} \quad (5)$$

Here, D is the stirrer diameter, T is the cell diameter, b is the blade height, and n_b is the number of impeller blades (Fig. 1A). The rotating Reynolds number is given by: $Re = \omega \rho_c D^2/(2\pi\eta_c)$, where ρ_c and η_c is the continuous phase density and viscosity, respectively, and ω is the angular velocity.

The boundary layer thickness, δ, is defined by the equation (Landau and Lifshitz, 1959):

$$\delta = \sqrt{\eta_c/(\rho_c \omega)} \quad (6)$$

The local shear stresses on the membrane surface are plotted in Figure 14. The maximum shear stress τ_{max} is expressed by putting r= r_{trans} in Eq. (3):

$$\tau_{max} = 0.825\, \eta_c \omega r_{trans} \frac{1}{\delta} \qquad (7)$$

The droplet diameter, x, can be predicted from a simple force balance on a droplet at pinch-off: $F_d = F_{ca}$, where F_{ca} and F_d are the capillary and drag force, respectively (Kosvintsev et al., 2005):

$$F_{ca} = \pi d_p \gamma \qquad (8)$$

$$F_d = 9\pi\tau x \sqrt{-r_p^2 + \left(\frac{x}{2}\right)^2} \qquad (9)$$

r_p is the pore radius and γ is the interfacial tension. Solving Eqs. (8) and (9) for x gives the equation for the drop diameter (Kosvintsev et al., 2005 and Stillwell et al., 2007):

$$x = \frac{\sqrt{18\tau^2 r_p^2 + 2\sqrt{81\tau^4 r_p^4 + 4 r_p^2 \tau^2 \gamma^2}}}{3\tau} \qquad (10)$$

Since the pressure on the surface of the membrane is lowest at $\tau=\tau_{max}$, the majority of the drops will be formed near the transitional radius and thus τ_{max} from Eq. (7) will be used instead of τ in Eq. (10).

References

Anastas, P. T., & Warner, J. C. Green Chemistry: Theory and Practice, Oxford University Press, New York, 1998.

Barnes, H. A. (1994). Rheology of emulsions—a review. Colloids and Surfaces A: Physicochemical and Engineering Aspects, 91, 89-95.

Brokel, U., Meier, W., & Wagner, G. Introduction. In: Brokel, U., Meier, W., & Wagner, G, editors. Product Design and Engineering. Vol. 1: Basics and Technologies. Weinheim: Wiley-VCH, 2007:1–3.

Castán, P., & González, X. Skin properties of glycerine polyethoxylene esters. In: Proceedings of 33th Annual Meeting of CED, Vol. 33. 2003:325–338.

Charcosset, C., Limayem, I., & Fessi, H. (2004). The membrane emulsification process—a review. Journal of chemical technology and biotechnology, 79(3), 209-218.

Cheetangdee, N., & Fukada, K. (2012). Protein stabilized oil-in-water emulsions modified by uniformity of size by premix membrane extrusion and their colloidal stability. Colloids and Surfaces A: Physicochemical and Engineering Aspects, 403, 54-61.

Cussler, E.L., & Moggridge, G.D. Chemical Product Design, 2nd ed. Cambridge, UK: Cambridge University Press, 2011.

Denolle, Y., Seita, V., & Delaire V. European Patents and Applications. EP 2368971 A1 20110928, 2011.

Dos Santos, R. G., Bannwart, A. C., Briceno, M. I., & Loh, W. (2011). Physico-chemical properties of heavy crude oil-in-water emulsions stabilized by mixtures of ionic and non-ionic ethoxylated nonylphenol surfactants and medium chain alcohols. Chemical Engineering Research and Design, 89(7), 957-967.

Dragosavac, M. M., Sovilj, M. N., Kosvintsev, S. R., Holdich, R. G., & Vladisavljević, G. T. (2008). Controlled production of oil-in-water emulsions containing unrefined pumpkin seed oil using stirred cell membrane emulsification. Journal of Membrane Science, 322(1), 178-188.

Egidi, E., Gasparini, G., Holdich, R. G., Vladisavljević, G. T., & Kosvintsev, S. R. (2008) Membrane emulsification using membranes of regular pore spacing: Droplet size and uniformity in the presence of surface shear. Journal of Membrane Science, 323(2), 414-420

Höfer, R., & Bigorra, J. (2007). Green chemistry—a sustainable solution for industrial specialties applications. Green Chemistry, 9(3), 203-212.

Karbstein, H., & Schubert, H. (1995). Developments in the continuous mechanical production of oil-in-water macro-emulsions. Chemical Engineering and Processing, 34(3), 205-211.

Kosvintsev, S. R., Gasparini, G., Holdich, R. G., Cumming, I. W., & Stillwell, M. T. (2005). Liquid-liquid membrane dispersion in a stirred cell with and without controlled shear. Industrial & Engineering Chemistry Research, 44(24), 9323-9330.

Kukizaki, M., & Goto, M. (2007). Preparation and evaluation of uniformly sized solid lipid microcapsules using membrane emulsification. Colloids and Surfaces A: Physicochemical and Engineering Aspects, 293(1-3), 87-94.

Landau, L. D., & Lifshitz, E. M. (1959). Fluid mechanics, 1959. Course of Theoretical Physics.

Lutz, P.J. Ca. Patents Applications.CA 2537554 A1 20060822, 2006.

Ma, G. (2003). Control of polymer particle size using porous glass membrane emulsification: A review. China Particuology, 1(3), 105-114.

McClements, D. J. Food Emulsions: Principles, Practice, and Techniques. Boca Raton: CRC Press, 2005.

Medvedovici, A., Udrescu, S., & David, V. (2013). Use of a green (bio) solvent–limonene–as extractant and immiscible diluent for large volume injection in the RPLC-tandem MS assay of statins and related metabolites in human plasma. Biomedical Chromatography, 27(1), 48-57.

Mezger, T. G. (2006). The rheology handbook: for users of rotational and oscillatory rheometers. Vincentz Network GmbH & Co KG.

Nagata, S. (1975). Mixing: principles and applications (Vol. 44). Tokyo: Kodansha.

Nazir, A., Schroën, K., & Boom, R. (2011). High-throughput premix membrane emulsification using nickel sieves having straight-through pores. Journal of Membrane Science, 383(1), 116-123.

Nazir, A., Schroën, K., & Boom, R. (2013). The effect of pore geometry on premix membrane emulsification using nickel sieves having uniform pores. Chemical Engineering Science, 93, 173-180.

Peng, S. J., & Williams, R. A. (1998). Controlled production of emulsions using a crossflow membrane: Part I: Droplet formation from a single pore. Chemical Engineering Research and Design, 76(8), 894-901.

Ramakrishnan, S., Ferrando, M., Aceña-Muñoz, L., De Lamo-Castellví, S., & Güell, C. (2013). Fish oil microcapsules from O/W emulsions produced by premix membrane emulsification. Food and Bioprocess Technology, 6(11), 3088-3101.

Santos, J., Trujillo-Cayado, L. A., Calero, N., & Muñoz, J. (2014). Physical characterization of eco-friendly O/W emulsions developed through a strategy based on product engineering principles. AIChE Journal. 60(7), 2644-2653.

Schubert, H., Ax, K., & Behrend, O. (2003). Product engineering of dispersed systems. Trends in Food Science & Technology, 14(1), 9-16.

Stillwell, M. T., Holdich, R. G., Kosvintsev, S. R., Gasparini, G., & Cumming, I. W. (2007). Stirred cell membrane emulsification and factors influencing dispersion drop size and uniformity. Industrial & Engineering Chemistry Research, 46(3), 965-972.

Suzuki, K., Fujiki, I., & Hagura, Y. (1998). Preparation of Corn Oil/Water and Water/Corn Oil Emulsions Using PTFE Membranes. Food Science and Technology International, Tokyo, 4(2), 164-167.

Suzuki, K., Shuto, I., & Hagura, Y. (1996). Characteristics of the Membrane Emulsification Method Combined with Preliminary Emulsification for Preparing Corn Oil-in-Water Emulsions. Food Science and Technology International, Tokyo, 2(1), 43-47.

Trujillo-Cayado, L. A., Ramírez, P., Pérez-Mosqueda, L. M., Alfaro, M. C., & Muñoz, J. (2014a). Surface and foaming properties of polyoxyethylene glycerol ester surfactants. Colloids and Surfaces A: Physicochemical and Engineering Aspects, 458(1), 195-202.

Trujillo-Cayado, L. A., Ramírez, Ruiz, M., Alfaro, M. C., & Muñoz, J. (2014b). Adsorption at the biocompatible -pinene–water interface and emulsifying properties of two eco-friendly surfactants. Colloids and Surfaces B: Biointerfaces, 122(1), 623-629

van Aken, G. A. (2002). Flow-induced coalescence in protein-stabilized highly concentrated emulsions. Langmuir, 18(7), 2549-2556.

van der Zwan, E., Schroen, K., van Dijke, K., & Boom, R. (2006). Visualization of droplet break-up in pre-mix membrane emulsification using microfluidic devices. Colloids and Surfaces A: Physicochemical and Engineering Aspects, 277(1-3), 223-229.

Vladisavljević, G. T., Shimizu, M., & Nakashima, T. (2004). Preparation of monodisperse multiple emulsions at high production rates by multi-stage premix membrane emulsification. Journal of Membrane Science, 244(1), 97-106.

Vladisavljević, G. T., Surh, J., & McClements, J. D. (2006). Effect of emulsifier type on droplet disruption in repeated Shirasu porous glass membrane homogenization. Langmuir, 22(10), 4526-4533.

Vladisavljević, G. T., Shimizu, M. & Nakashima, T. (2006b). Production of multiple emulsions for drug delivery systems by repeated SPG membrane homogenization: Influence of mean pore size, interfacial tension and continuous phase viscosity. Journal of Membrane Science, 284(1-2), 373-383.

Walter J. (2010). Metabolism of terpenoids in animal models and humans. In: Husnu Can Baser K, Buchbauer, G., editors. Handbook of essential oils: Science, Technology and Applications. Boca Raton: CRC Press, 209-232.

Yafei, W., Tao, Z., & Gang, H. (2006). Structural evolution of polymer-stabilized double emulsions. Langmuir, 22(1), 67-73.

Yuan, Q., Williams, R. A., & Biggs, S. (2009). Surfactant selection for accurate size control of microcapsules using membrane emulsification. Colloids and Surfaces A: Physicochemical and Engineering Aspects, 347(1), 97-103.

Zhou, Q. Z., Ma, G. H., & Su, Z. G. (2009). Effect of membrane parameters on the size and uniformity in preparing agarose beads by premix membrane emulsification. Journal of Membrane Science, 326(2), 694-700.

Figure 1

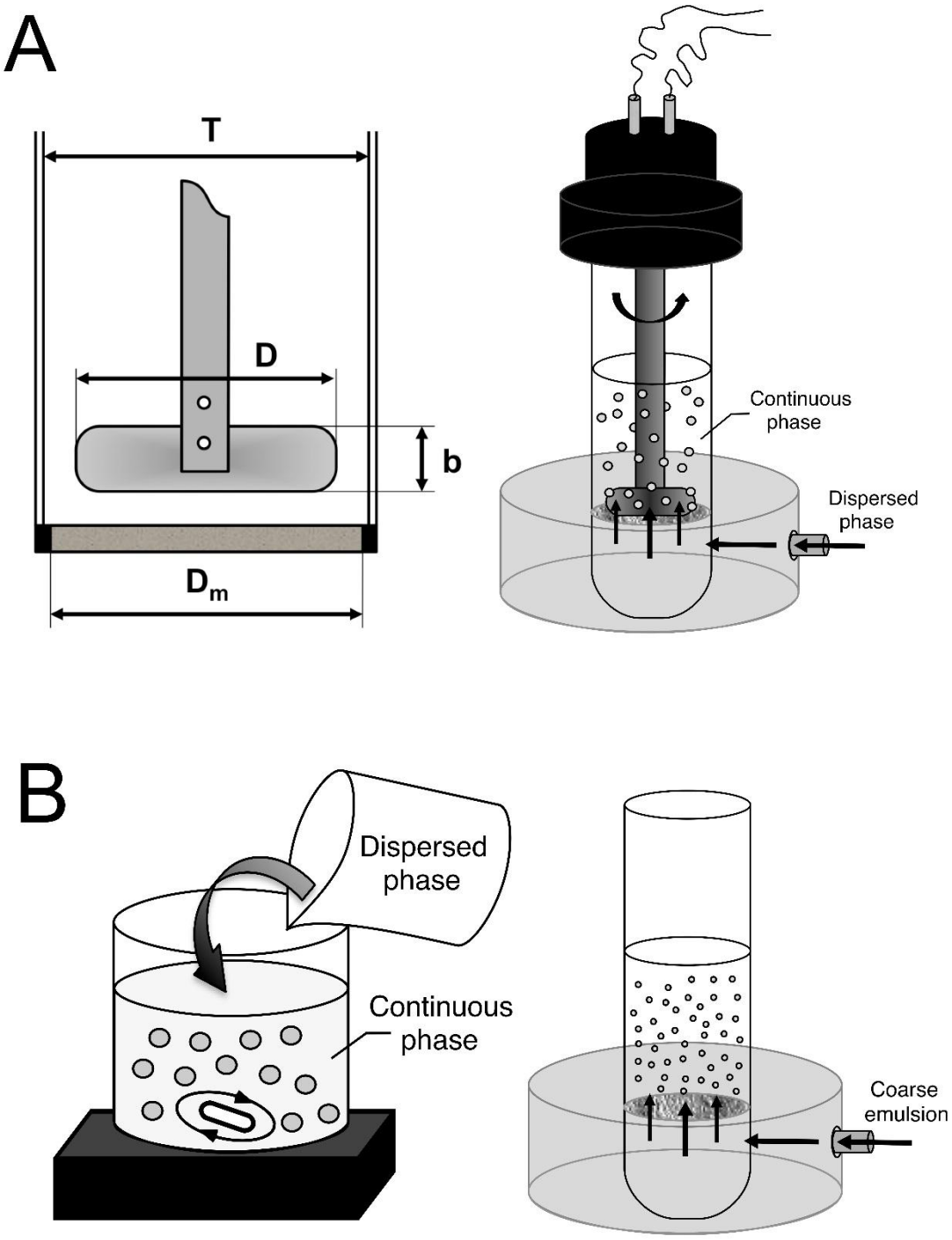

Figure 1. A) Schematic illustration of Dispersion Cell with simple paddle stirrer above a flat-disc membrane (b= 11 mm, D= 30 mm, D_m= 32 mm, and T= 37 mm) used in direct ME. B) Schematic illustration of the premix ME process used. The coarse emulsion was prepared by magnetic stirrer and injected through the membrane without stirring.

Figure 2

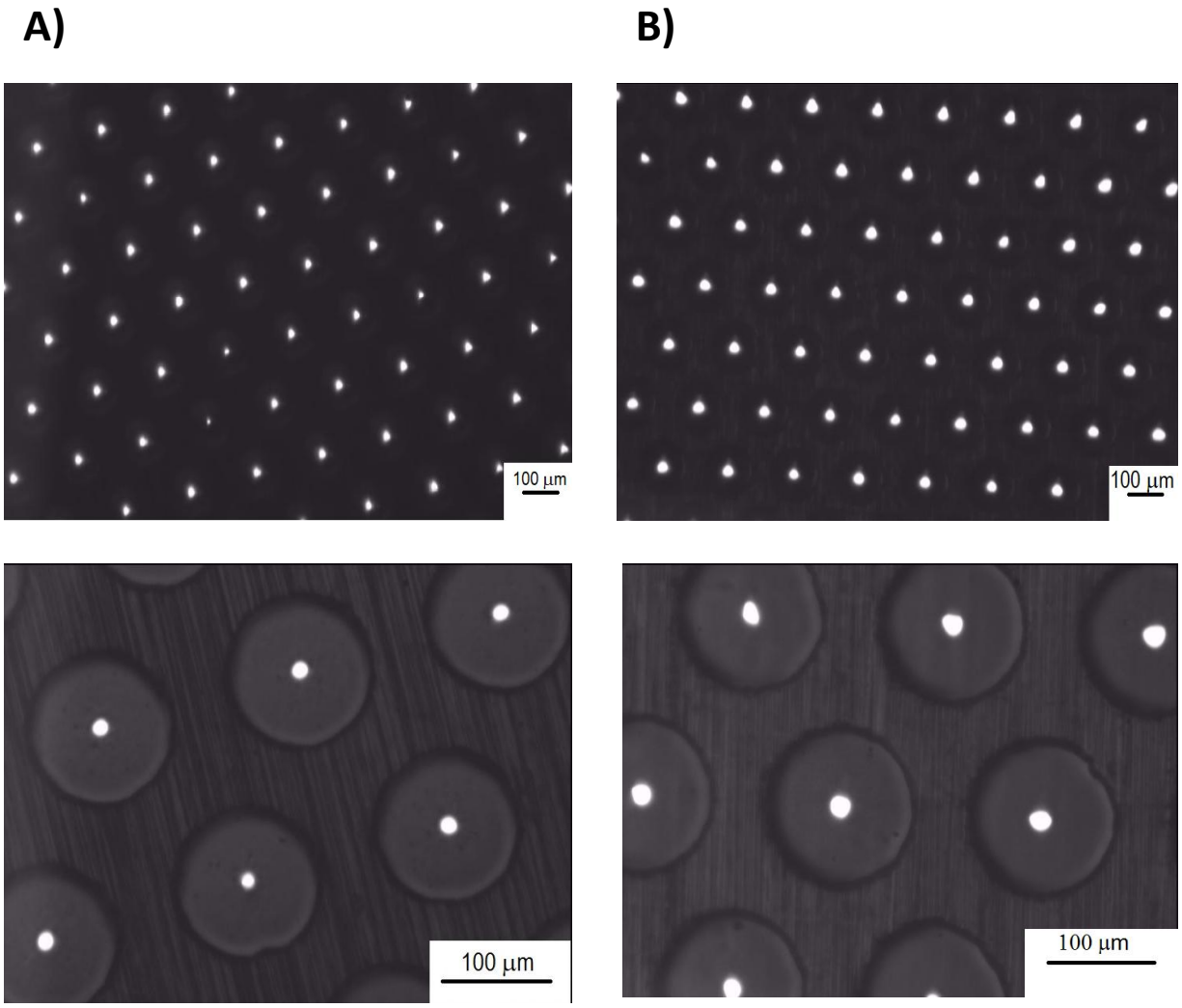

Figure 2. Photomicrographs of the membrane surface taken at two different magnifications: A) 10 µm pore size membrane and B) 20 µm pore size membrane.

Figure 3

A)

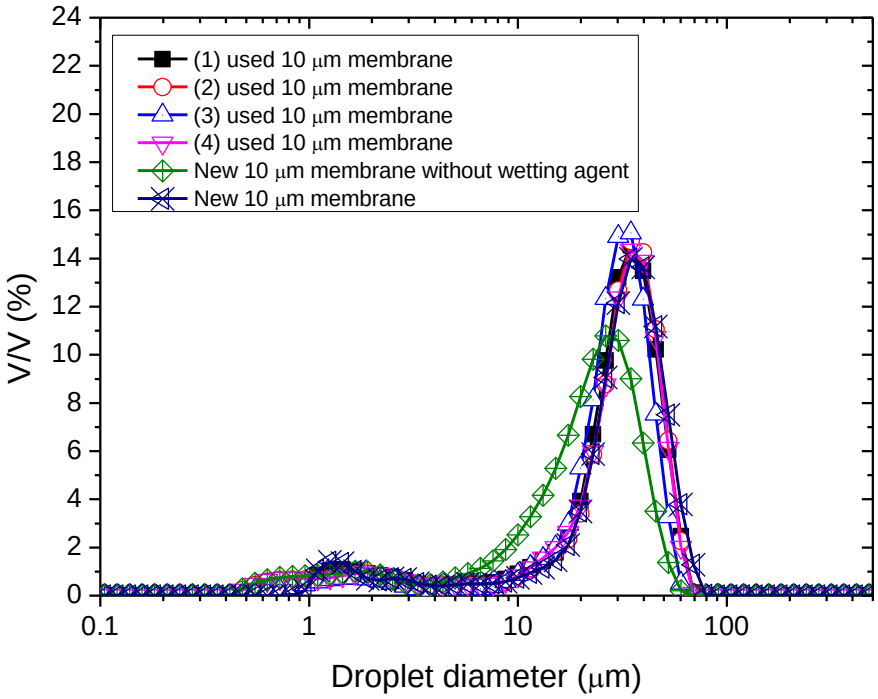

B)

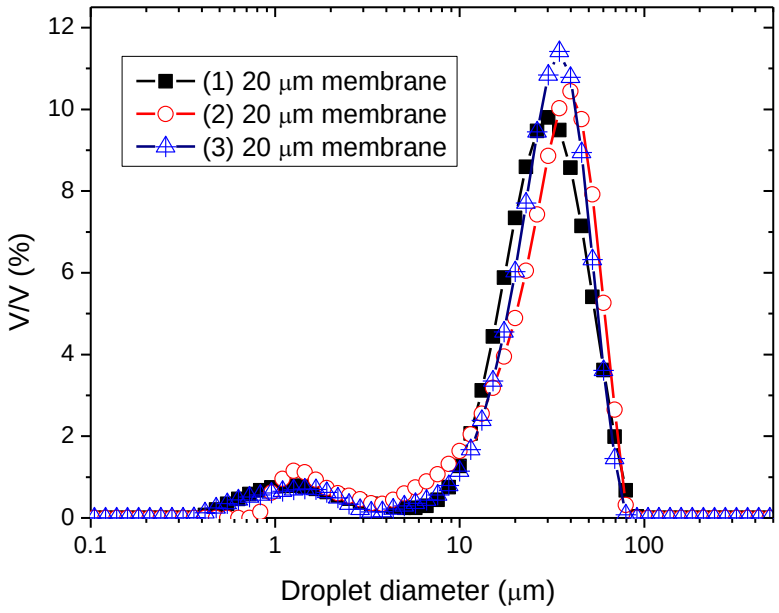

Figure 3. Particle size distribution of emulsions in repeated runs: A) 25/75 emulsion produced using direct ME at 850 rpm and 600 L m^{-2} h^{-1} with a 10 μm membrane and B) 25/75 emulsion produced using single-pass premix ME at 706 L m^{-2} h^{-1} with a 20 μm membrane.

Figure 4

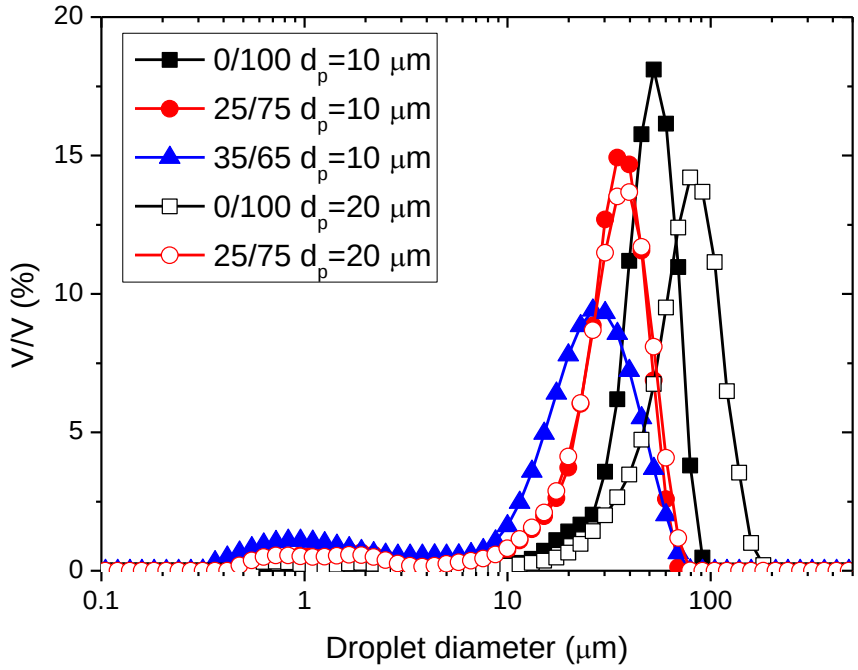

Figure 4. PSD for emulsions prepared by direct ME at 620 rpm and 600 L m^{-2} h^{-1} as a function of the pore size of the membrane and the ratio of solvents in the dispersed phase.

Figure 5

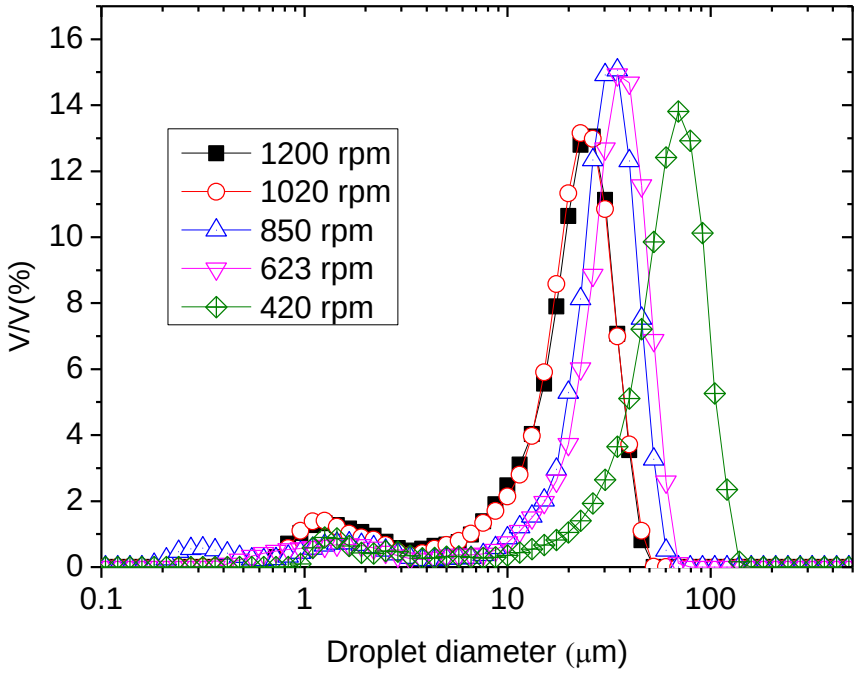

Figure 5. The effect of stirring speed on the PSD of 25/75 emulsions prepared by direct ME at 600 L m^{-2} h^{-1} with a 10 μm membrane.

Figure 6

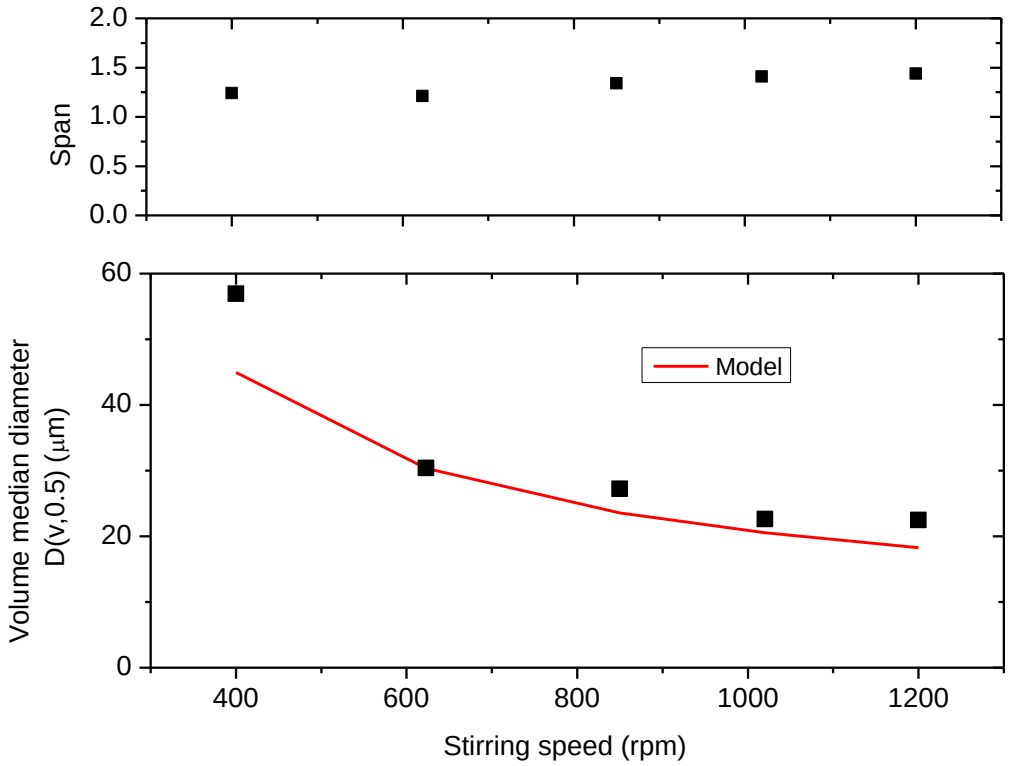

Figure 6. The volume median diameter, D(v, 0.5) and span of the emulsions prepared by direct ME at 600 L m^{-2} h^{-1} with a 10 μm membrane as a function of stirring speed. The predicted droplet diameters are calculated using analytical model presented in the appendix A.

Figure 7

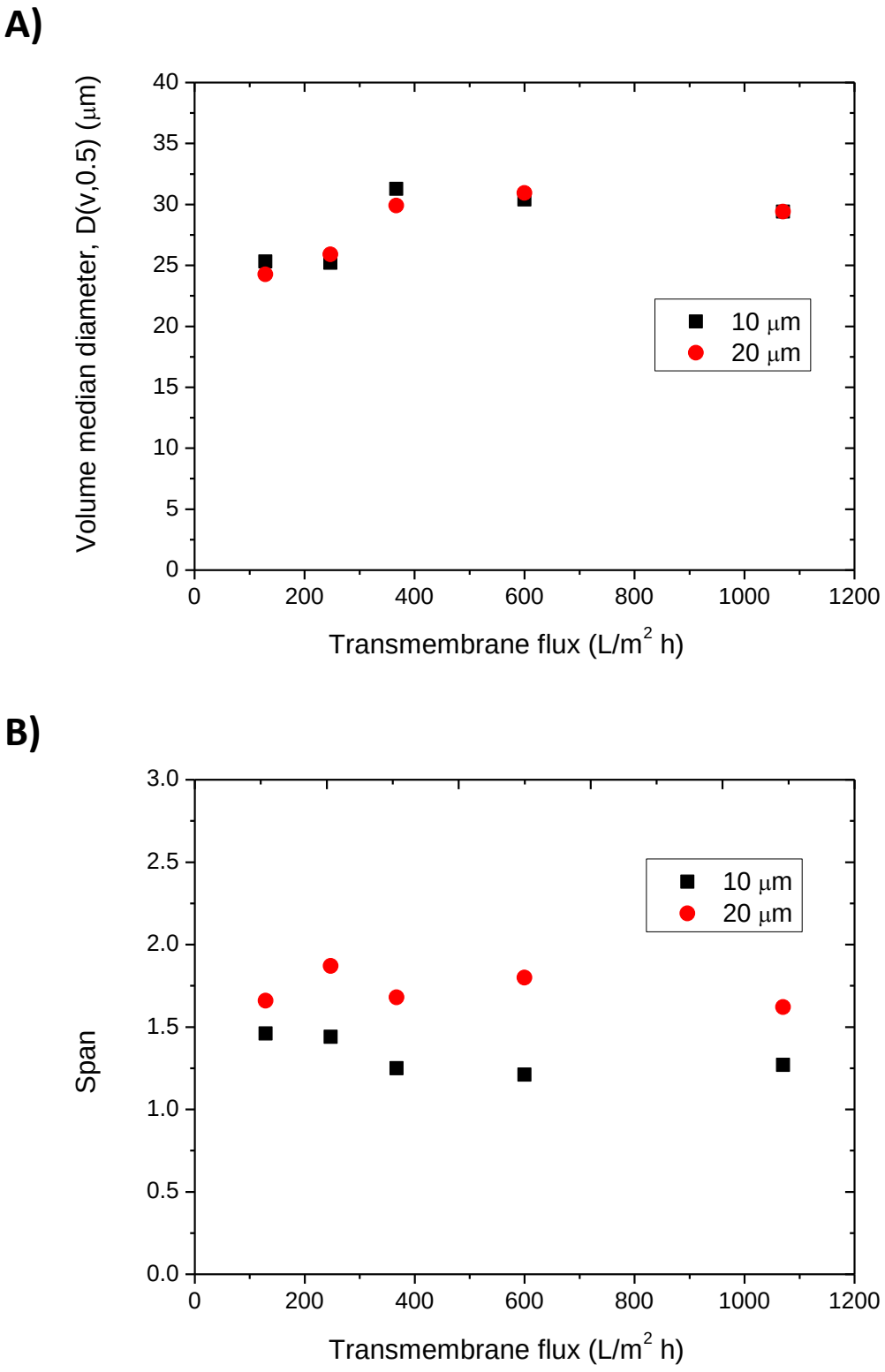

Figure 7. The effect of transmembrane flux on: A) Volume median diameter, D(v,0.5) and B) Span for the emulsions processed by direct ME at 620 rpm with a 10 and 20 μm membrane.

Figure 8

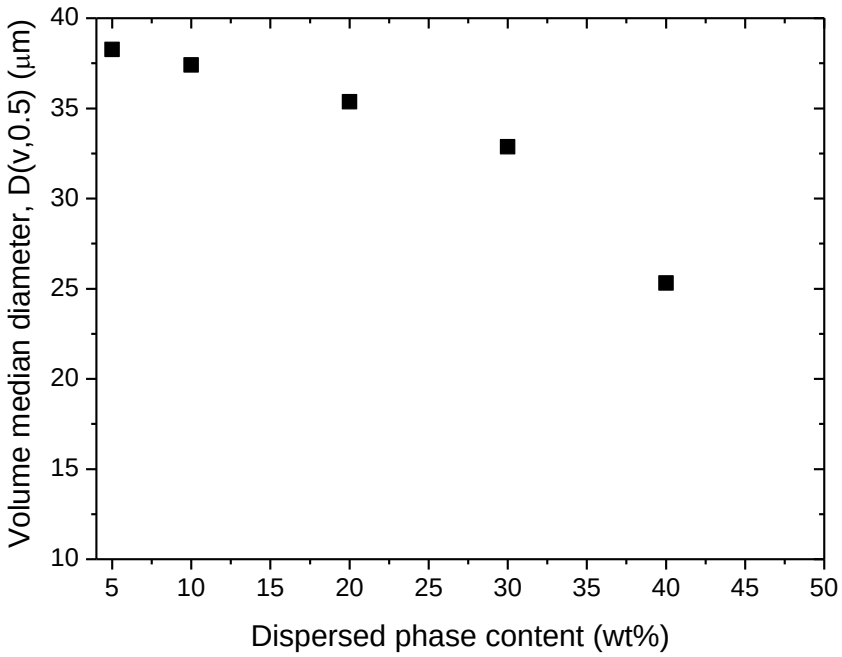

Figure 8. The effect of the dispersed phase content in the emulsions on the volume mean diameter, (D(v,0.5) in direct ME at 129 L m^{-2} h^{-1} and 620 rpm with 10 μm membrane. The surfactant/oil ratio was kept at 0.10 (w/w) in all samples.

Figure 9

(A)

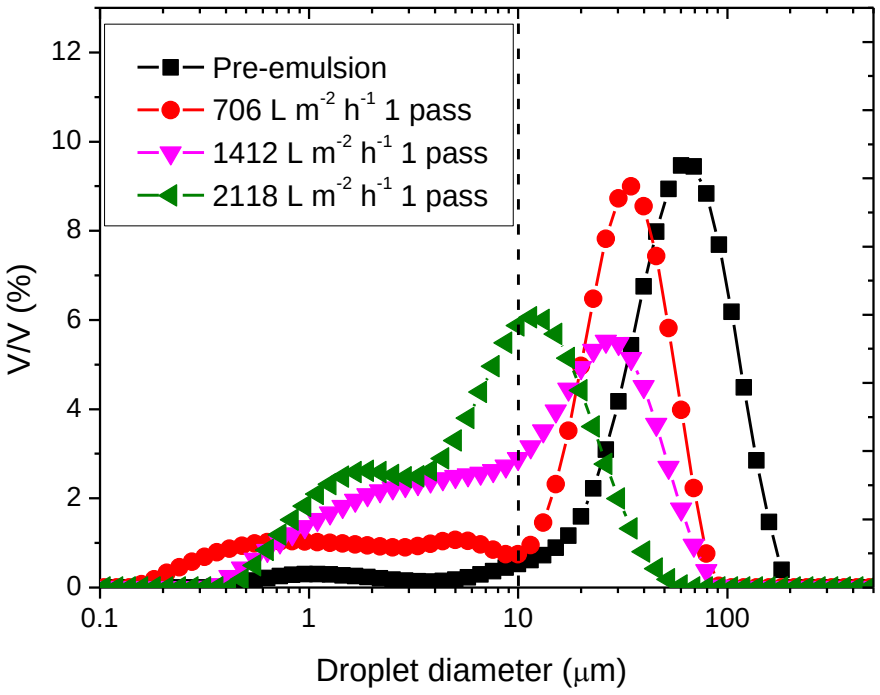

(B)

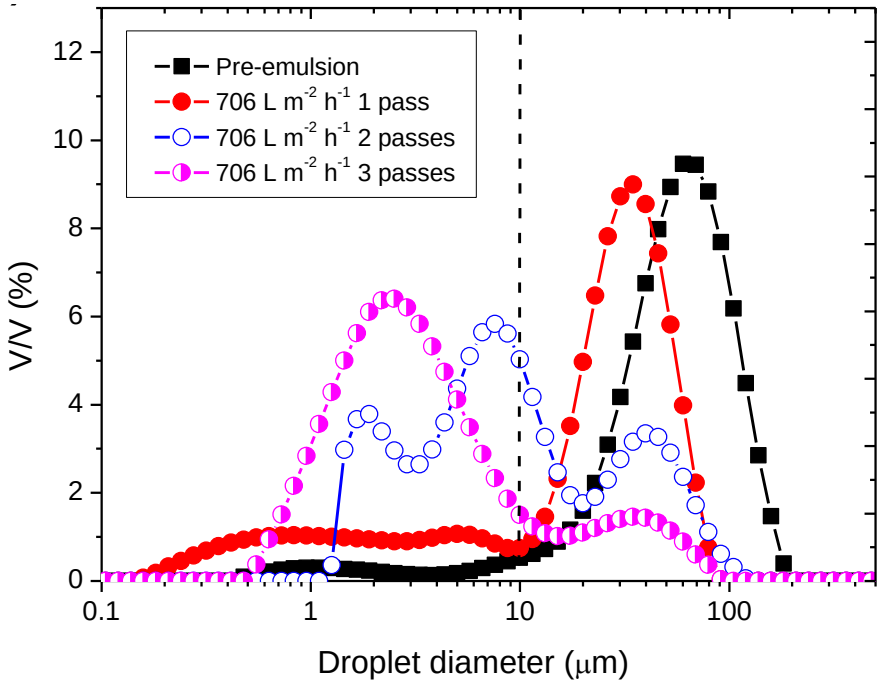

Figure 9. The effect of transmembrane flux (A) and number of membrane passes (B) on the PSD of the emulsions prepared by premix ME using a 10 μm membrane. The location of the dashed line corresponds to the membrane pore diameter.

Figure 10

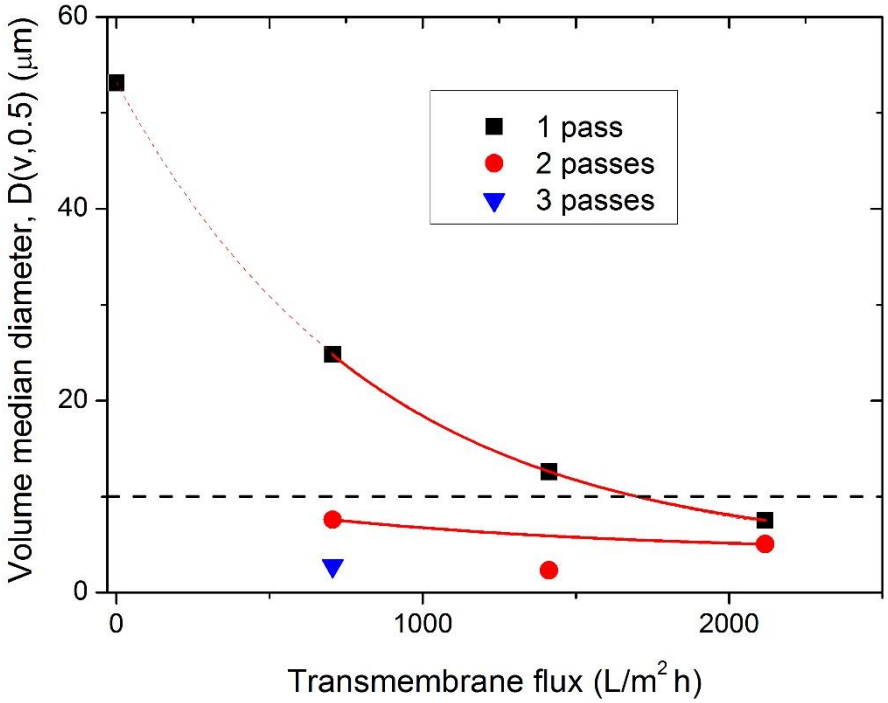

Figure 10. The effect of transmembrane flux and number of passes through the 10 μm membrane on the volume median diameter of emulsions prepared by premix ME.

Figure 11

(A)

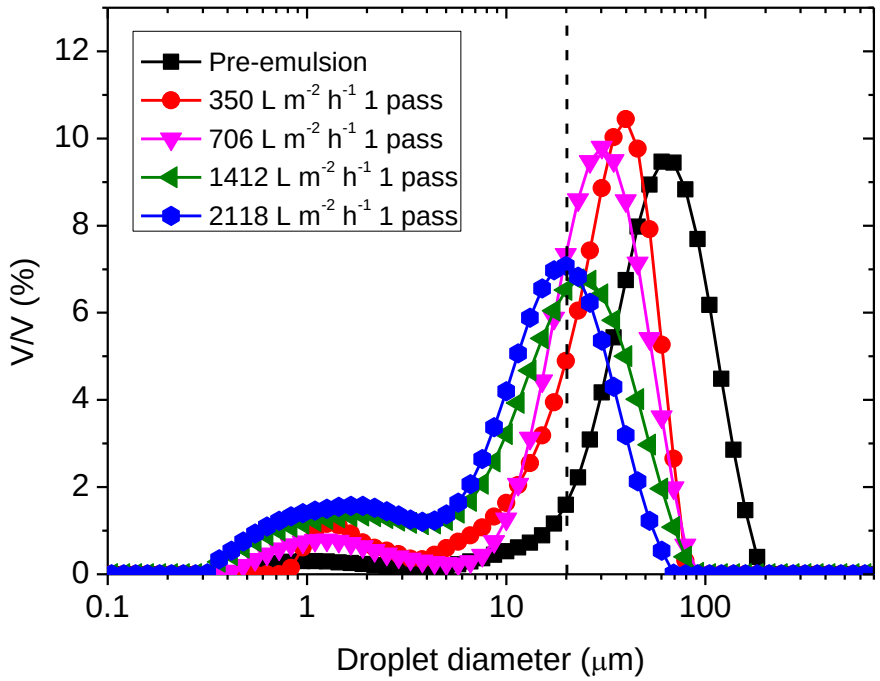

(B)

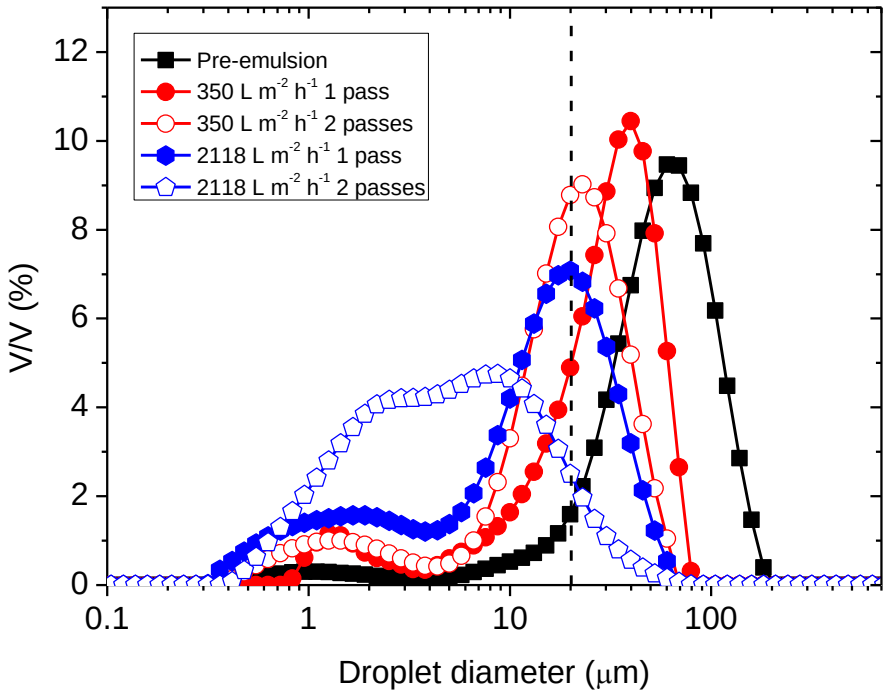

Figure 11. The effect of transmembrane flux (A) and number of passes through the membrane (B) on the PSD of emulsions obtained by premix ME with the 20 μm pore size membrane.

Figure 12

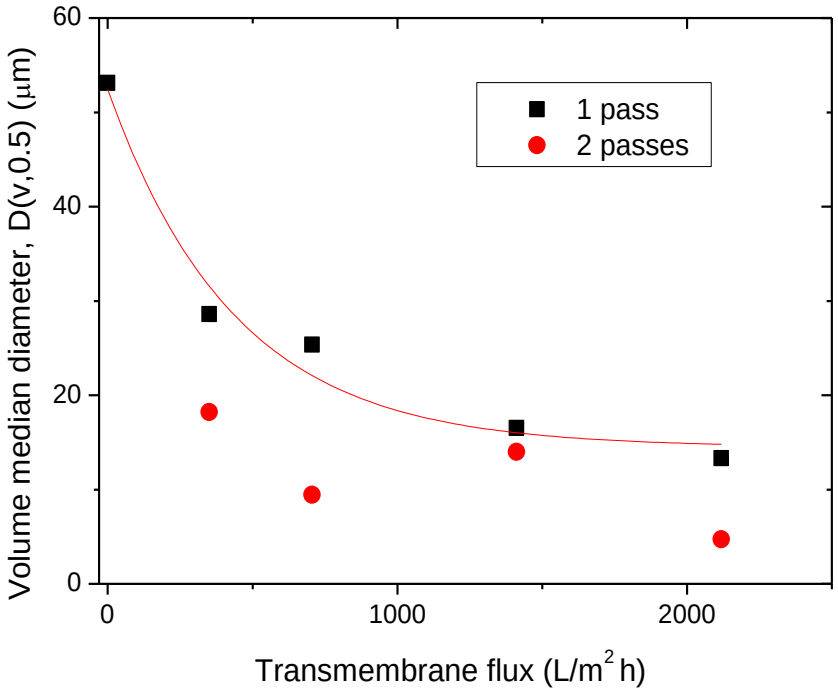

Figure 12. The effect of transmembrane flux and number of passes through the membrane on D(v,0.5) for emulsions obtained by premix ME using the 20 μm pore size membrane.

Figure 13

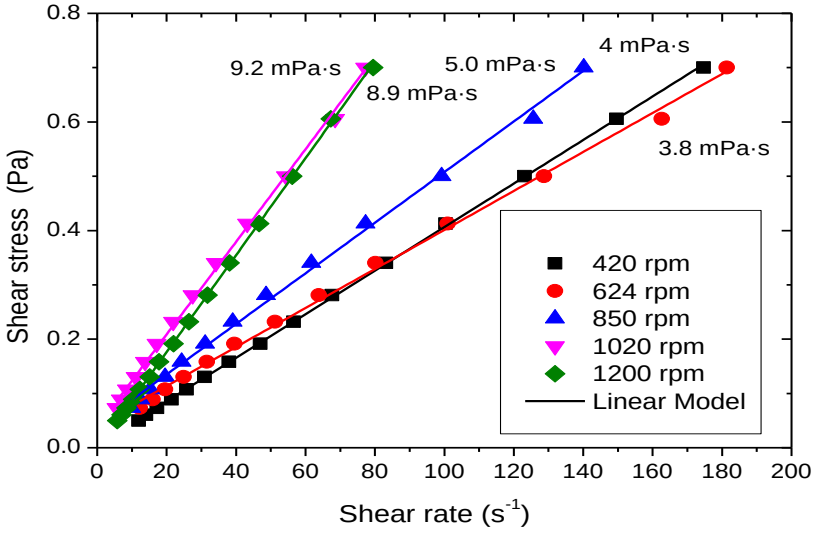

Fig. 13A. The effect of stirring speed on the flow curves for the emulsions produced by direct ME at 600 L m^{-2} h^{-1} using 10 µm membrane. Straight lines are the best fit lines.

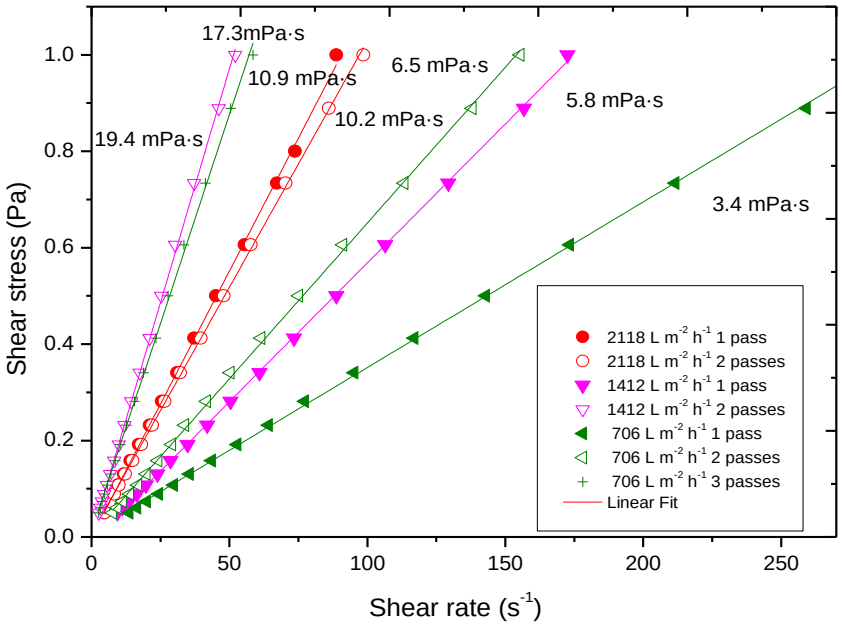

Fig. 13B. The effect of transmembrane flux on flow curves for the emulsions produced by premix ME using 10 µm membrane. Straight lines are the best fit lines.

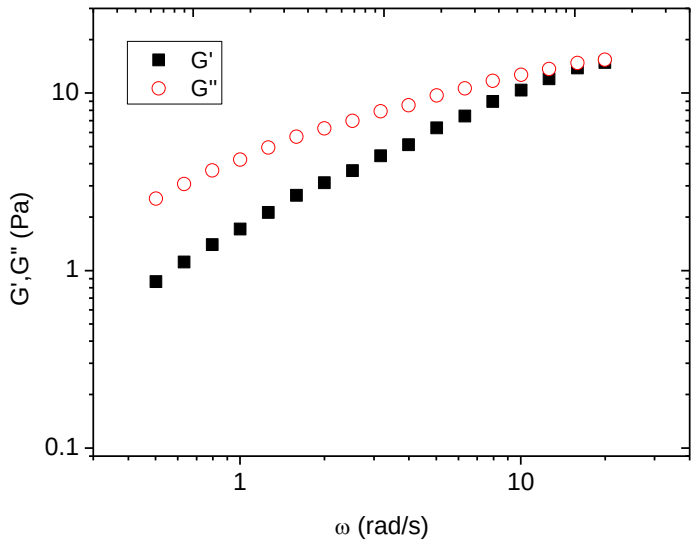

Figure 13C. Mechanical spectra for 40 wt% emulsion produced by direct ME at 129 L m^{-2} h^{-1} and 620 rpm using 10 µm membrane.

Figure 14

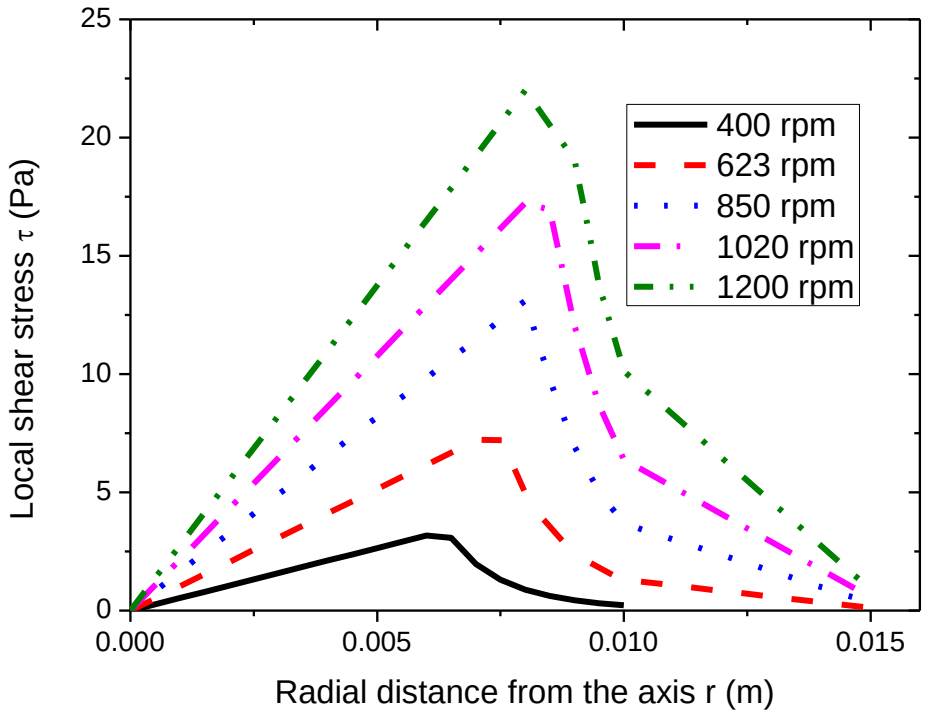

Figure 14. The variation of local shear stress over the membrane surface at different stirrer speeds for 30% emulsion, calculating using Eq. (3) or Eq. (4).

Table 1

Table 1. The effect of the ratio of AMD-10 and d-limonene in the dispersed phase on the volume median diameter and span for emulsions prepared by direct ME at 620 rpm and 600 L m^{-2} h^{-1}.

wt% AMD-10 in dispersed phase	10 µm membrane		20 µm membrane	
	D(v,0.5)	span	D(v,0.5)	span
0	45.5	0.9	69.3	1.1
25	30.4	1.2	30.9	1.2
35	21.7	1.8	-	-

Table 2

Table 2. The equilibrium interfacial tension between the aqueous and oil phase for different solvent ratios in the absence and in the presence of the used surfactant at 20^{o}C.

AMD-10/d-limonene mass ratio (wt/wt)	**Interfacial tension (mN m^{-1})**	
	no surfactant	3 wt% Levenol ® C-201
0/100	40.0 ± 1.3	7.0 ± 0.5
25/75	7.0 ± 0.4	1.0 ± 0.1
35/65	4.0 ± 0.3	-